2017 IEEE Conference on Control Technology and Applications (CCTA)
August 27-30, 2017. Kohala Coast, Hawai'i, USA

Convex Optimization of a Spacecraft Stabilization with a Double-Gimbal Variable-Speed Control Moment Gyro Actuator: Geometric Approach*

Takahiro Sasaki[1], Hanspeter Schaub[2] and Takashi Shimomura[3]

Abstract— **This paper applies the linear parameter-varying (LPV) control theory to the attitude stabilization problem for a spacecraft with a double-gimbal variable-speed control moment gyro (DGVSCMG). The LPV control theory can provide an optimal gain-scheduled (GS) controller by using linear matrix inequalities (LMIs) with regional pole placement constraints. When LMIs are solved, most studies select a common Lyapunov function for the whole operating range. However, selecting a common Lyapunov function leads to conservatism of design. The scheduling parameters in the LPV model of a spacecraft with a DGVSCMG have an interesting property. By using this property, this paper proposes the method to geometrically reduce the number of vertices in the convex hull to cover the LPV system. Through numerical examples, the proposed method can reduce the conservatism of design.**

I. INTRODUCTION

Control moment gyros (CMGs) have been used for 3-axis attitude control of spacecraft as attitude actuators. CMGs are capable of producing large gyroscopic control torques onto the spacecraft which are proportional to the rotor speed and the gimbal rate. A double-gimbal variable-speed CMG (DGVSCMG) has two gimbal axes and a variable speed wheel. A DGVSCMG can generate large three dimensional torques if the wheel motor torque is sized accordingly. This advantage enables a high-speed attitude maneuver. Some studies related to DGVSCMGs are discussed in References [1], [2], [3]. In particular, Stevenson and Schaub [1] develop the spacecraft-DGVSCMG dynamics and presented a nonlinear control algorithm with a Newton-Raphson (NR) scheme. Zhang and Fang [2] apply robust backstepping control while considering disturbance torques to the attitude control problem by using a DGVSCMG. Further, Jikuya et al. [3] show two types of computational procedures for a rest-to-rest maneuver using a DGVSCMG.

The satellite dynamics with a DGVSCMG is described through a set of nonlinear differential equations. Most of recent studies about attitude control have used non-linear controllers such as Lyapunov function-based controllers [4], [5]. With Lyapunov function-based controllers, overall stability of attitude control is always guaranteed. However, the closed-loop control performance is not discussed in detail. To study the DGVSCMG performance, the linear parameter-varying (LPV) control theory [6] is applied to the attitude stabilization problems. In the LPV control theory, to avoid difficulties coming from the nonlinearity in satellite dynamics, the dynamics of spacecraft is modeled as an LPV system. A gain-scheduled (GS) controller is applied to this model using linear matrix inequalities (LMIs) [7], [8].

A variety of control problems have been solved via LMIs under common Lyapunov functions [6], [7], [9], [10]. Regarding GS control as in [6], which can be considered for some class of nonlinear systems which can be described as LPV, if one selects a common Lyapunov function for a whole operating range, the overall stability of the closed-loop system as time varying is guaranteed for any changing rate of the scheduling variable. However, selecting a common Lyapunov function for the whole operating range leads to conservatism of design. Many researchers have judged that this conservatism arises from selecting a common Lyapunov function and shifted their research into parameter dependent Lyapunov functions [11], [12], [13], [14]. However, theory of parameter dependent Lyapunov functions are more complicated and sometimes installed additional sufficient conditions or a line search parameter to make the problem convex. In addition, changing rates of scheduling variables are restricted in many cases. As a result, it has not been so useful for practitioners to use so far. To avoid such conservatism easily, the post-guaranteed LMI method [15] and another method [16], in which the distinct Lyapunov solutions are adopted. Another method to reduce the conservatism of solving the LMIs are to reduce the number of vertices of the convex hull with the operation range of the system [17], [18], [19] or to divide the convex hull [20], [21].

In this study, first, the dynamics of a spacecraft with a DGVSCMG is developed. Then, an interesting characteristic of the scheduling parameters of a DGVSCMG is focused on and the proposed method to reduce the vertices of the convex hull is adopted by geometric approach. Finally, a GS controller is designed by using LMIs for $\mathcal{H}_2$ constraints and regional pole placement [16], [22] and the effectiveness is demonstrated by numerical simulation results.

*This work was supported by by JSPS Grant-in-Aid for Scientific Research Grant Numbers 15J11371 and (C)15K06149.

[1]Takahiro Sasaki is Graduate Student at the Department of Aerospace Engineering, Osaka Prefecture University, Sakai Osaka 599-8531, Japan and Visiting Scholar at University of Colorado Boulder, Colorado 80309, USA aero2021@gmail.com

[2]Hanspeter Schaub is Alfred T. and Betty E. Look Professor at the Department of Aerospace Engineering Science, Colorado Center for Astrodynamics Research, University of Colorado Boulder, Colorado 80309, USA hanspeter.schaub@colorado.edu

[3]Takashi Shimomura is Professor at the Department of Aerospace Engineering, Osaka Prefecture University, Sakai Osaka 599-8531, Japan shimomura@aero.osakafu-u.ac.jp

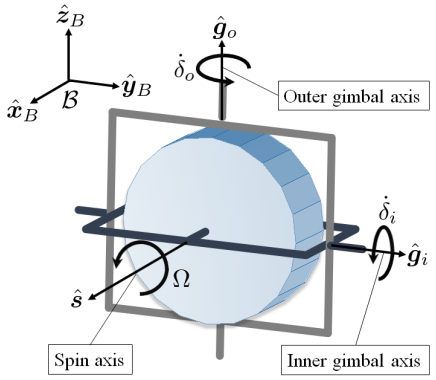

Fig. 1. DGVSCMG.

II. EQUATION OF MOTION

The spacecraft considered in this paper is assumed to be a rigid body and contains a single DGVSCMG device. The body-fixed frame $\mathcal{B}$ is represented by a set of unit vectors $\hat{\boldsymbol{x}}_B$, $\hat{\boldsymbol{y}}_B$, and $\hat{\boldsymbol{z}}_B$. The inertial frame is given by $\mathcal{N}$. Symbol $\mathcal{G}_o, \mathcal{G}_i$, and $\mathcal{W}$ denote the outer gimbal axis frame, the inner gimbal axis frame, and the wheel spin axis frame, respectively. Then, as in Fig. 1, the unit vectors of the spin axis, the inner gimbal axis, and the outer gimbal axis are denoted by $\hat{\boldsymbol{s}}$, $\hat{\boldsymbol{g}}_i$, and $\hat{\boldsymbol{g}}_o$, respectively. The outer gimbal axis $\hat{\boldsymbol{g}}_o$ is always paralleled to $\hat{\boldsymbol{z}}_B$ of the body frame $\mathcal{B}$. Therefore, it is given as follows:

$$ {}^{\mathcal{B}}\hat{\boldsymbol{g}}_o = {}^{\mathcal{B}}\begin{bmatrix} 0 \\ 0 \\ 1 \end{bmatrix}, \; {}^{\mathcal{B}}\hat{\boldsymbol{g}}_i = {}^{\mathcal{B}}\begin{bmatrix} -\sin\delta_o \\ \cos\delta_o \\ 0 \end{bmatrix}, \; {}^{\mathcal{B}}\hat{\boldsymbol{s}} = {}^{\mathcal{B}}\begin{bmatrix} \cos\delta_o\cos\delta_i \\ \sin\delta_o\cos\delta_i \\ -\sin\delta_i \end{bmatrix} $$

where δ_i, δ_o denote the inner and outer gimbal angles, respectively. The dynamics of a spacecraft with a DGVSCMG [1] is considered. The total inertial angular momentum $\boldsymbol{H}$ is described by

$$ \boldsymbol{H} = \boldsymbol{H}_B + \boldsymbol{H}_{go} + \boldsymbol{H}_{gi} + \boldsymbol{H}_{ws} \tag{1} $$

with

$$ \boldsymbol{H}_B = [I_s]\boldsymbol{\omega}_{\mathcal{B}/\mathcal{N}} \tag{2a} $$
$$ \boldsymbol{H}_{go} = [I_{go}]\boldsymbol{\omega}_{\mathcal{G}_o/\mathcal{N}} \tag{2b} $$
$$ \boldsymbol{H}_{gi} = [I_{gi}]\boldsymbol{\omega}_{\mathcal{G}_i/\mathcal{N}} \tag{2c} $$
$$ \boldsymbol{H}_{ws} = [I_{ws}]\boldsymbol{\omega}_{\mathcal{W}/\mathcal{N}} \tag{2d} $$

where

$$ \boldsymbol{\omega}_{\mathcal{G}_o/\mathcal{N}} = \boldsymbol{\omega}_{\mathcal{B}/\mathcal{N}} + \dot{\delta}_o\hat{\boldsymbol{g}}_o \tag{3a} $$
$$ \boldsymbol{\omega}_{\mathcal{G}_i/\mathcal{N}} = \boldsymbol{\omega}_{\mathcal{B}/\mathcal{N}} + \dot{\delta}_o\hat{\boldsymbol{g}}_o + \dot{\delta}_i\hat{\boldsymbol{g}}_i \tag{3b} $$
$$ \boldsymbol{\omega}_{\mathcal{W}/\mathcal{N}} = \boldsymbol{\omega}_{\mathcal{B}/\mathcal{N}} + \dot{\delta}_o\hat{\boldsymbol{g}}_o + \dot{\delta}_i\hat{\boldsymbol{g}}_i + \Omega\hat{\boldsymbol{s}} \tag{3c} $$

and $[I_s]$ is the inertia matrix of a spacecraft excluding DGVSCMG inertia contributions and $\boldsymbol{\omega}_{\mathcal{B}/\mathcal{N}}$ is the inertial angular velocity of the spacecraft. $[I_{gi}]$ and $[I_{go}]$ are the moment of inertia of the DGVSCMG about the inner and outer gimbal axis, respectively; $[I_{ws}]$ is the moment of inertia of the wheel about the spin axis; and Ω is the wheel spin rate. The total inertia matrix $[J]$ of a spacecraft including a DGVSCMG device is given by

$$ [J] = [I_s] + [I_{go}] + [I_{gi}] + [I_{ws}]. \tag{4} $$

Note that this inertia tensor $[J]$ will vary with time as seen by the body frame. Assuming that no external torque is applied to the spacecraft body, the dynamics is given by

$$ \dot{\boldsymbol{H}} = \boldsymbol{0}. \tag{5} $$

Substituting Eq. (1) into the first term of the LHS in Eq. (5) yields

$$ \dot{\boldsymbol{H}}_B + \dot{\boldsymbol{H}}_{go} + \dot{\boldsymbol{H}}_{gi} + \dot{\boldsymbol{H}}_{ws} = \boldsymbol{0}. \tag{6} $$

In the following development, the short-hand notation $\boldsymbol{\omega} = \boldsymbol{\omega}_{\mathcal{B}/\mathcal{N}}$ is used to make equation description more compact. Similarly, gimbal frame angular velocity definitions are shortened such as $\boldsymbol{\omega}_{\mathcal{G}_o/\mathcal{N}} = \boldsymbol{\omega}_{go}$, $\boldsymbol{\omega}_{\mathcal{G}_o/\mathcal{N}} = \boldsymbol{\omega}_{gi}$, and $\boldsymbol{\omega}_{\mathcal{W}/\mathcal{N}} = \boldsymbol{\omega}_{ws}$. Taking the inertial time derivative of the first term of the LHS in Eq. (6) leads to

$$ \dot{\boldsymbol{H}}_B = [I_s]\dot{\boldsymbol{\omega}} + \boldsymbol{\omega}^{\times}[I_s]\boldsymbol{\omega}. \tag{7} $$

In the sequel, the notation $\boldsymbol{x}^{\times}$ denotes the following skew-symmetric matrix:

$$ \boldsymbol{x}^{\times} := \begin{bmatrix} 0 & -x_3 & x_2 \\ x_3 & 0 & -x_1 \\ -x_2 & x_1 & 0 \end{bmatrix}, \quad {}^{\forall}\boldsymbol{x} = [x_1 \; x_2 \; x_3]^T. \tag{8} $$

The second term of the LHS in Eq. (6) is shown as follows:

$$ \dot{\boldsymbol{H}}_{go} = [I_{go}](\dot{\boldsymbol{\omega}} + \ddot{\delta}_o\hat{\boldsymbol{g}}_o + \boldsymbol{\omega}^{\times}(\dot{\delta}_o\hat{\boldsymbol{g}}_o)) + \boldsymbol{\omega}_{go}^{\times}([I_{go}]\boldsymbol{\omega}_{go}) \tag{9} $$

The third term of the LHS in Eq. (6) is related to the inner gimbal of the DGVSCMG. This is shown as follows:

$$ \begin{aligned} \dot{\boldsymbol{H}}_{gi} = [I_{gi}](\dot{\boldsymbol{\omega}} + \ddot{\delta}_o\hat{\boldsymbol{g}}_o + \ddot{\delta}_i\hat{\boldsymbol{g}}_i + \boldsymbol{\omega}^{\times}(\dot{\delta}_o\hat{\boldsymbol{g}}_o + \dot{\delta}_i\hat{\boldsymbol{g}}_i) + \\ (\dot{\delta}_i\hat{\boldsymbol{g}}_i)^{\times}(\dot{\delta}_o\hat{\boldsymbol{g}}_o)) + \boldsymbol{\omega}_{gi}^{\times}([I_{gi}]\boldsymbol{\omega}_{gi}) \end{aligned} \tag{10} $$

The fourth term of the LHS in Eq. (6) is related to the wheel spin rate of the DGVSCMG. This is shown as follows:

$$ \begin{aligned} \dot{\boldsymbol{H}}_{ws} = [I_{ws}](\dot{\boldsymbol{\omega}} + \ddot{\delta}_o\hat{\boldsymbol{g}}_o + \ddot{\delta}_i\hat{\boldsymbol{g}}_i + \dot{\Omega}\hat{\boldsymbol{s}} + \boldsymbol{\omega}^{\times}(\dot{\delta}_o\hat{\boldsymbol{g}}_o + \dot{\delta}_i\hat{\boldsymbol{g}}_i \\ + \Omega\hat{\boldsymbol{s}}) + (\dot{\delta}_o\hat{\boldsymbol{g}}_o)^{\times}(\dot{\delta}_i\hat{\boldsymbol{g}}_i + \Omega\hat{\boldsymbol{s}}) + (\dot{\delta}_i\hat{\boldsymbol{g}}_i)^{\times}(\Omega\hat{\boldsymbol{s}})) \\ + \boldsymbol{\omega}_{ws}^{\times}([I_{ws}]\boldsymbol{\omega}_{ws}) \end{aligned} \tag{11} $$

Substituting Eqs. (7)-(11) into Eq. (6), the dynamics of a spacecraft with a DGVSCMG is obtained.

III. LPV MODELING

An LPV model to design GS controllers for attitude stabilization is developed. First, Eq. (6) must be transformed into an LPV model that linearly depends on scheduling parameters [6]. The Jacobian linearization of Eq. (6) around the equilibrium point ($\boldsymbol{\omega}_{eq} = 0$, $\dot{\Omega}_{eq} = 0$, $\dot{\delta}_{i_{eq}} = 0$, $\dot{\delta}_{o_{eq}} = 0$) leads to the linear dynamics of a spacecraft with a DGVSCMG as follows:

$$ \dot{\boldsymbol{\omega}} = \boldsymbol{A}(\boldsymbol{\rho})\boldsymbol{\omega} + \boldsymbol{B}(\boldsymbol{\rho})\boldsymbol{u} + \boldsymbol{E}w \tag{12} $$

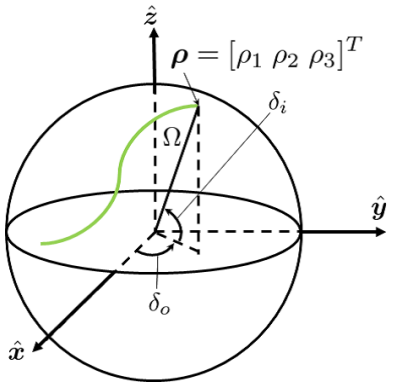

Fig. 2. Operation range of a DGVSCMG.

where $\boldsymbol{u} = [\dot{\Omega}\ \dot{\delta}_i\ \dot{\delta}_o]^T$ is the control input, $\boldsymbol{E}w$ the disturbance term including model error and

$$\boldsymbol{A}(\boldsymbol{\rho}) = [J]^{-1}[I_{ws}]\boldsymbol{M}(\boldsymbol{\rho}), \tag{13}$$

$$\boldsymbol{B}(\boldsymbol{\rho}) = -[J]^{-1}[I_{ws}]\boldsymbol{N}(\boldsymbol{\rho}), \tag{14}$$

with

$$\begin{aligned}\boldsymbol{M}(\boldsymbol{\rho}) &= (\Omega\hat{\boldsymbol{s}})^{\times} \\ &= \begin{bmatrix} 0 & \Omega\sin\delta_i & \Omega\cos\delta_i\sin\delta_o \\ -\Omega\sin\delta_i & 0 & -\Omega\cos\delta_i\cos\delta_o \\ -\Omega\cos\delta_i\sin\delta_o & \Omega\cos\delta_i\cos\delta_o & 0 \end{bmatrix}\end{aligned} \tag{15}$$

$$\begin{aligned}\boldsymbol{N}(\boldsymbol{\rho}) &= [\hat{\boldsymbol{s}}\ \ \Omega\hat{\boldsymbol{g}}_i\times\hat{\boldsymbol{s}}\ \ \Omega\hat{\boldsymbol{g}}_o\times\hat{\boldsymbol{s}}] \\ &= \begin{bmatrix} \cos\delta_i\cos\delta_o & -\Omega\sin\delta_i\cos\delta_o & -\Omega\cos\delta_i\sin\delta_o \\ \cos\delta_i\sin\delta_o & -\Omega\sin\delta_i\sin\delta_o & \Omega\cos\delta_i\cos\delta_o \\ -\sin\delta_i & -\Omega\cos\delta_i & 0 \end{bmatrix}\end{aligned} \tag{16}$$

where $\boldsymbol{\rho}(\Omega\ \delta_i\ \delta_o)$ is the scheduling parameter vector. If $\boldsymbol{\rho}$ is defined by $\boldsymbol{\rho} = [\Omega\ \ \sin\delta_i\ \ \cos\delta_i\ \ \sin\delta_o\ \ \cos\delta_o]^T$, this system is covered with a convex hull which has 32 $(= 2^5)$ extreme points or vertices [6]. In this way, the scheduling parameters of the LPV model in Eq. (12) have too many vertices to perform the GS controller design. To overcome this problem, the method is considered to reduce the number of vertices. The part which depends on the scheduling parameters of the coefficient matrix $\boldsymbol{B}(\boldsymbol{\rho})$ is embeded into a new input $\boldsymbol{u}'$ as follows:

$$\bar{\boldsymbol{B}} = -[J]^{-1}[I_{ws}] \tag{17}$$

$$\boldsymbol{u}' = \boldsymbol{N}(\boldsymbol{\rho})\boldsymbol{u} \tag{18}$$

Therefore, the state-space representation of Eq. (12) is rewritten as follows:

$$\dot{\boldsymbol{\omega}} = \boldsymbol{A}(\boldsymbol{\rho})\boldsymbol{\omega} + \bar{\boldsymbol{B}}\boldsymbol{u}' + \boldsymbol{E}w \tag{19}$$

In this case, it is easy to design the optimal GS controller to define the scheduling parameters as follows:

$$\boldsymbol{\rho} = \begin{bmatrix} \Omega\hat{\boldsymbol{s}}_1 \\ \Omega\hat{\boldsymbol{s}}_2 \\ -\Omega\hat{\boldsymbol{s}}_3 \end{bmatrix} = \begin{bmatrix} \Omega\cos\delta_i\cos\delta_o \\ \Omega\cos\delta_i\sin\delta_o \\ \Omega\sin\delta_i \end{bmatrix} := \begin{bmatrix} \rho_1 \\ \rho_2 \\ \rho_3 \end{bmatrix} \tag{20}$$

In this case, matrix $\boldsymbol{M}(\boldsymbol{\rho})$ in Eq. (15) is rewritten by

$$\boldsymbol{M}(\boldsymbol{\rho}) = \begin{bmatrix} 0 & \rho_3 & \rho_2 \\ -\rho_3 & 0 & -\rho_1 \\ -\rho_2 & \rho_1 & 0 \end{bmatrix}. \tag{21}$$

Therefore, the scheduling parameters of a spacecraft with a DGVSCMG in Eq. (20) have an interesting property. It can be represented by the spherical coordinate system as in Fig. 2. This property comes from DGVSCMG's motion. Note that the wheel spin rate Ω represents the radial coordinate and the gimbal angles δ_i and δ_o represent the angular coordinate.

IV. CONVEX OPTIMIZATION

To design the GS controller, the convex hull to cover the LPV system is designed.

A. Convex Hull #1

The polytopic system is introduced. Setting the state variable $\boldsymbol{x} := \boldsymbol{\omega}$, the state-space representation of Eq. (19) is described as follows:

$$\dot{\boldsymbol{x}} = \boldsymbol{A}(\boldsymbol{\rho})\boldsymbol{x} + \bar{\boldsymbol{B}}\boldsymbol{u}' + \boldsymbol{E}w \tag{22}$$

With the maximum value and the minimum one of the scheduling parameters, the number of vertices is set to 8 $(= 2^3)$. The coefficient matrix in this LPV system can be expressed by the following polytopic representation:

$$\boldsymbol{A}(\boldsymbol{\rho}) = \sum_{i=1}^{8}\lambda_i(\boldsymbol{\rho})\boldsymbol{A}_{ei},\ \ \lambda_i(\boldsymbol{\rho}) \geq 0,\ \ \sum_{i=1}^{8}\lambda_i(\boldsymbol{\rho}) = 1 \tag{23}$$

Let $\underline{\rho}_i$ and $\overline{\rho}_i$ denote the lower and the upper bound of ρ_i. Using these parameters and introducing the following interpolation parameters $\underline{\alpha}_i$ and $\overline{\alpha}_i$, the scheduling parameters ρ_i can be described as follows:

$$\rho_i = \underline{\alpha}_i\underline{\rho}_i + \overline{\alpha}_i\overline{\rho}_i, \quad 0 \leq \underline{\alpha}_i,\ \overline{\alpha}_i \leq 1, \quad \underline{\alpha}_i + \overline{\alpha}_i = 1 \tag{24}$$

In this way, this system is covered with the convex hull as in Fig. 3. From Eq. (20), the operation range of the scheduling parameter is given by

$$-\Omega_{max} \leq \rho_1 \leq \Omega_{max}; \tag{25}$$

$$-\Omega_{max} \leq \rho_2 \leq \Omega_{max}; \tag{26}$$

$$-\Omega_{max} \leq \rho_3 \leq \Omega_{max}. \tag{27}$$

Therefore, first, the extreme controller $\boldsymbol{K}_i$ is designed at each vertex of the convex hull. Then, the GS controller $\boldsymbol{K}(\boldsymbol{\rho})$ is obtained by the combination of those extreme controllers as follows:

$$\boldsymbol{K}(\boldsymbol{\rho}) = \sum_{i=1}^{8}\lambda_i(\boldsymbol{\rho})\boldsymbol{K}_i,\ \ \lambda_i(\boldsymbol{\rho}) \geq 0,\ \ \sum_{i=1}^{8}\lambda_i(\boldsymbol{\rho}) = 1. \tag{28}$$

B. Convex Hull #2

How to reduce the vertex of the convex hull is considered. Setting the new scheduling parameters

$$-\Omega_{max} \leq \rho_1' \leq (1+\sqrt{2})\Omega_{max}; \tag{29}$$

$$-\Omega_{max} \leq \rho_2' \leq (1+\sqrt{2})\Omega_{max}; \tag{30}$$

$$-\Omega_{max} \leq \rho_3' \leq \Omega_{max}, \tag{31}$$

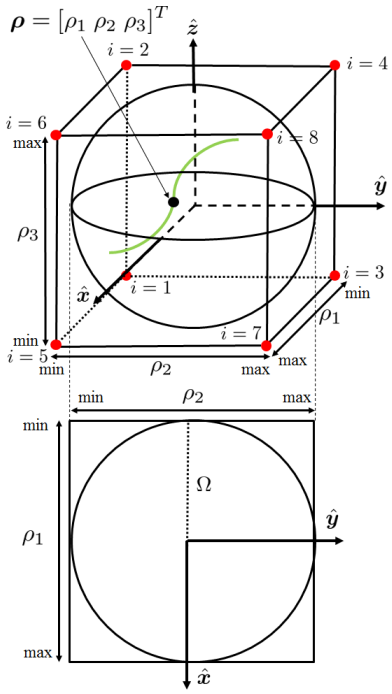

Fig. 3. Convex hull #1.

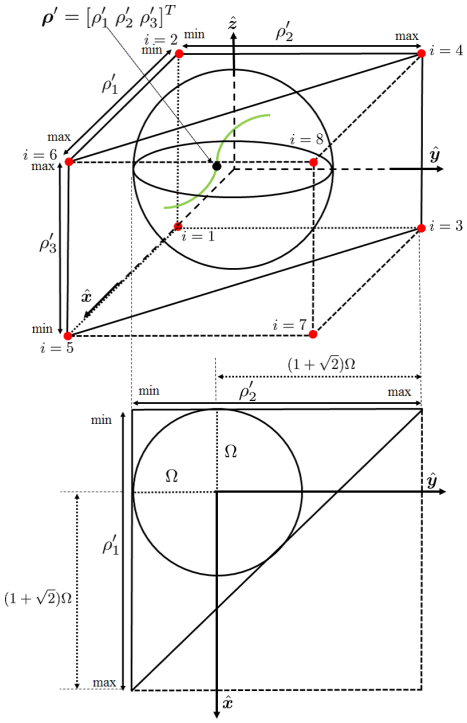

Fig. 4. Convex hull #2.

the system is covered with the convex hull as in Fig. 4. In this case, the number of the vertex can be represented by 8 or 6 and the polytopic representation $\boldsymbol{A}(\boldsymbol{\rho})$ is given by

$$\boldsymbol{A}(\boldsymbol{\rho}') = \sum_{i=1}^{n} \lambda_i(\boldsymbol{\rho}')\boldsymbol{A}_{ei},\ \ \lambda_i(\boldsymbol{\rho}') \geq 0,\ \ \sum_{i=1}^{n} \lambda_i(\boldsymbol{\rho}) = 1. \quad (32)$$

Similary, the GS controller $\boldsymbol{K}(\boldsymbol{\rho})$ is obtained by the combination of extreme controllers as follows:

$$\boldsymbol{K}(\boldsymbol{\rho}') = \sum_{i=1}^{n} \lambda_i(\boldsymbol{\rho}')\boldsymbol{K}_i,\ \ \lambda_i(\boldsymbol{\rho}') \geq 0,\ \ \sum_{i=1}^{n} \lambda_i(\boldsymbol{\rho}) = 1. \quad (33)$$

Note that n denotes the number of vertices in this case 8 or 6. The vertices ($i = 1,\ 2$) are common in convex hull #1 or #2 as in Figs. 3 and 4.

V. MULTIOBJECTIVE CONTROLLER DESIGN

A GS controller with LMIs that guarantees overall stability and achieves $\mathcal{H}_2$ performance for the LPV model as in Eq. (22) is considered. First, the generalized plant for Eq. (22) is defined as follows:

$$\begin{cases} \dot{\boldsymbol{x}} = \boldsymbol{A}(\tilde{\boldsymbol{\rho}})\boldsymbol{x} + \bar{\boldsymbol{B}}\boldsymbol{u}' + \boldsymbol{E}\boldsymbol{w} \\ \boldsymbol{z} = \boldsymbol{C}\boldsymbol{x} + \boldsymbol{D}\boldsymbol{u}' \end{cases} \quad (34)$$

where $\tilde{\boldsymbol{\rho}}$ is set to $\boldsymbol{\rho}$ in Eq. (25) or $\boldsymbol{\rho}'$ in Eq. (29) and the coefficient matrix set $(\boldsymbol{C}, \boldsymbol{D})$ is normally selected such that they satisfy the condition $\boldsymbol{C}^T\boldsymbol{D} = 0$, $\boldsymbol{D}^T\boldsymbol{D} > 0$, and where $\boldsymbol{w}$ and $\boldsymbol{z}$ are the disturbance input vector and the performance output vector, respectively. In this study, LMI representation for pole placement[16], [22] is introduced as well as LMIs for $\mathcal{H}_2$ performance. The following LMI problem is considered:

$$\inf_{\boldsymbol{W}_i, \boldsymbol{X}, \boldsymbol{Z}} [\text{Trace } (\boldsymbol{Z})] \quad \text{subject to}$$

$$\begin{bmatrix} \boldsymbol{X} & * \\ \boldsymbol{E}^T & \boldsymbol{Z} \end{bmatrix} > 0, \quad (35)$$

$$\begin{bmatrix} (\boldsymbol{A}_i\boldsymbol{X} - \bar{\boldsymbol{B}}\boldsymbol{W}_i) + (\ \bullet\ )^T & * \\ \boldsymbol{C}\boldsymbol{X} - \boldsymbol{D}\boldsymbol{W}_i & -\boldsymbol{I} \end{bmatrix} < 0, \quad (36)$$

$$(\boldsymbol{A}_i\boldsymbol{X} - \bar{\boldsymbol{B}}\boldsymbol{W}_i) + (\ \bullet\ )^T + 2\alpha\boldsymbol{X} < 0, \quad (37)$$

$$\begin{bmatrix} -r\boldsymbol{X} & \boldsymbol{A}_i\boldsymbol{X} - \bar{\boldsymbol{B}}\boldsymbol{W}_i \\ * & -r\boldsymbol{X} \end{bmatrix} < 0, \quad (38)$$

$$\begin{bmatrix} \boldsymbol{\Phi}_i\ (\Theta) & \boldsymbol{\Psi}_i\ (\Theta) \\ * & \boldsymbol{\Phi}_i\ (\Theta) \end{bmatrix} < 0, \quad (39)$$

for all $1 \leq i \leq p$,

where

$$\boldsymbol{\Phi}_i\ (\Theta) = \sin\Theta\left\{(\boldsymbol{A}_i\boldsymbol{X} - \bar{\boldsymbol{B}}\boldsymbol{W}_i) + (\ \bullet\ )^T\right\} \quad (40)$$

$$\boldsymbol{\Psi}_i\ (\Theta) = \cos\Theta\left\{(\boldsymbol{A}_i\boldsymbol{X} - \bar{\boldsymbol{B}}\boldsymbol{W}_i) - (\ \bullet\ )^T\right\} \quad (41)$$

and p is the number of scheduling parameters, in this case p is set to 8 or 6. Note that Eqs. (35) and (36) present the $\mathcal{H}_2$ norm constraint and Eqs. (37)-(39) present the regional pole constraints [16], [22] as in Fig. 2. Using the optimal solution sets $\boldsymbol{X}$, $\boldsymbol{W}_i$ to the problem in Eqs. (35)-(39), the extreme controllers are given as follows:

$$\boldsymbol{K}_i = \boldsymbol{W}_i\boldsymbol{X}^{-1}, \quad 1 \leq i \leq p. \quad (42)$$

Substituting Eq. (42) into Eq. (28) or (33), the GS controller $\boldsymbol{K}(\boldsymbol{\rho})$ is given by

$$\boldsymbol{u}' = -\boldsymbol{K}(\boldsymbol{\rho})\boldsymbol{x}. \quad (43)$$

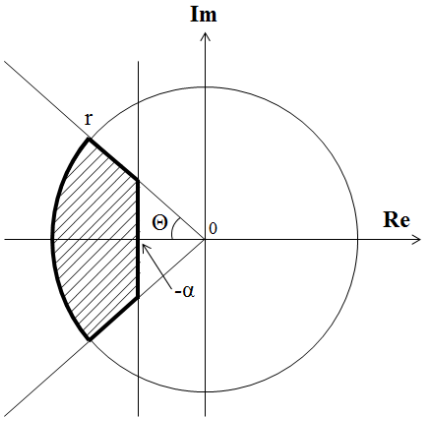

Fig. 5. Pole Placement.

VI. NUMERICAL SIMULATIONS

This section presents two numerical simulations by using two types convex hulls (with 8 vertices or 6 vertices). The controller design parameters $\boldsymbol{C}$ and $\boldsymbol{D}$, and the disturbance coefficient matrix $\boldsymbol{E}$ are given as follows:

$$\boldsymbol{C} = \begin{bmatrix} 30 \times \boldsymbol{I}_3 \\ \boldsymbol{0}_{3\times 3} \end{bmatrix}, \quad \boldsymbol{D} = \begin{bmatrix} 0_{3\times 3} \\ 0.01 \times \boldsymbol{I}_3 \end{bmatrix}, \quad \boldsymbol{E} = \begin{bmatrix} \boldsymbol{I}_3 \\ 0_{3\times 3} \end{bmatrix} \quad (44)$$

The simulation parameters are given in Table I, in which the initial condition, the minimum input or the maximum one of the DGVSCMG are given.

Figure 6 shows the time histories of the $\mathcal{H}_2$ norms (the evaluation function of the LQ problem J_{zw}) in Cases 1-3. The function J_{zw} is defined as follows:

$$J_{zw}(t) = \int_0^t (\boldsymbol{x}^T \boldsymbol{C}^T \boldsymbol{C} \boldsymbol{x} + \boldsymbol{u}^T \boldsymbol{D}^T \boldsymbol{D} \boldsymbol{u}) d\tau \quad (45)$$

Note that the terminating time of the $\mathcal{H}_2$ norm is considered as the current time. The number of vertex and volume of two convex hulls are shown in Table II.

Figure 7 shows the angular velocity of a spacecraft and DGVSCMG's motion by using convex hull #1 in Case 1. From this figure, attitude stabilization of a spacecraft is successfully accomplished. From Fig. 6, the proposed GS controller with 6 vertices has improved the control performance compared with the GS controller with 8 vertices. From this Table and simulation results, in attitude control of a spacecraft with DGVSCMG, the effectiveness of the convex hull with few vertices is demonstrated.

VII. CONCLUSIONS

This paper, first, presents the dynamics and the linear parameter-varying (LPV) model of a spacecraft with a double-gimbal variable-speed control moment gyro (DGVSCMG). Then two types of convex hull are proposed while focusing on the characteristics of the scheduling parameters in the LPV model. To design optimal gain-scheduled (GS) controllers, linear matrix inequalities (LMIs) with regional pole placement constraints are applied. Finally, the simulation results demonstrate the effectiveness of the convex hull with few vertices.

TABLE I
SIMULATION PARAMETERS.

Parameter	value	Unit
$[J]$	diag[10 10 8]	kgm^2
$[I_{ws}]$	diag[0.008 0.008 0.008]	kgm^2
$[I_{gi}]$	diag[0.001 0.001 0.001]	kgm^2
$[I_{go}]$	diag[0.001 0.001 0.001]	kgm^2
Ω_0	200	rad/s
Ω_{max}	300	rad/s
$\dot{\Omega}_{min},\ \dot{\Omega}_{max}$	$-5,\ 5$	$\mathrm{rad/s}^2$
$\delta_{i0},\ \delta_{o0}$	$0,\ 0$	rad
$\dot{\delta}_{i,min},\ \dot{\delta}_{i,max}$	$-1,\ 1$	rad/s
$\dot{\delta}_{o,min},\ \dot{\delta}_{o,max}$	$-1,\ 1$	rad/s
$\boldsymbol{\omega}_0$ (Case 1)	$[0.08\ 0.05\ -0.06]$	rad/s
$\boldsymbol{\omega}_0$ (Case 2)	$[-0.02\ 0.04\ -0.08]$	rad/s
$\boldsymbol{\omega}_0$ (Case 3)	$[-0.08\ -0.06\ -0.05]$	rad/s

TABLE II
COMPARISON OF TWO CONVEX HULLS (CHS).

-	CH #1	CH #2	
Vertices	8	6	8
Volume ($\times\Omega_{max}^3$)	8	$6+4\sqrt{2}$	$12+8\sqrt{2}$

REFERENCES

[1] D. Stevenson and H. Schaub, "Nonlinear Control Analysis of a Double-Gimbal Variable-Speed Control Moment Gyroscope," *Journal of Guidance, Control, and Dynamics,* Vol. 35, No. 3, pp. 787-793, 2012.

[2] H. Zhang and J. Fang, "Robust Backstepping Control for Agile Satellite Using Double-Gimbal Variable-Speed Control Moment Gyroscope," *Journal of Guidance, Control, and Dynamics*, Vol. 36, No. 5, pp. 1356-1363, 2013.

[3] I. Jikuya, K. Fujii, and K. Yamada, "Attitude Maneuver of Spacecraft with a Variable-Speed Double-Gimbal Control Mmoment Gyro," *Advances in Space Research,* Vol. 58, No. 7, pp. 1303-1317, 2016.

[4] P. Tsiotras, "Stabilization and Optimality Results for the Attitude Control Problem," *Journal of Guidance, Control, and Dynamics*, Vol. 19, No. 4 , pp. 772-779, 1996.

[5] H. Yoon and P. Tsiotras, "Spacecraft Line-of-Sight Control Using a Single Variable-Speed Control Moment Gyro," *Journal of Guidance, Control, and Dynamics*, Vol. 29, No. 6, pp. 1295-1308, 2006.

[6] P. Apkarian, P. Gahinet, and G. Becker, "Self-Scheduled $\mathcal{H}_\infty$ Control of Linear Parameter-Varying Systems: A Design Example," *Automatica*, Vol. 31, No. 9, pp. 1251-1261, 1995.

[7] S. Boyd, E. L. Ghaoui, E. Feron, and V. Balakrishnan, *Linear Matrix Inequalities in System and Control Theory*, Volume 15 of Studies in Applied Mathematics, Society for Industrial and Applied Mathematics (SIAM), 1994.

[8] J. C. Geromel, P. L. D. Peres, and J. Bernussou, "On a Convex Parameter Space Method for Linear Control Design of Uncertain Systems," *SIAM Journal on Control and Optimization*, Vol. 29, No. 2, pp. 381-402, 1991.

[9] I. Masubuchi, A. Ohara, and N. Suda, "LMI-based controller synthesis: A unified formulation and solution," *Int. J. Robust Nonlin. Contr.*, vol. 8, no. 8, pp. 669-686, 1998.

[10] C. Scherer, P. Gahinet, and M. Chilali, "Multiobjective outputfeedback control via LMI optimization," *IEEE Trans. on Automat. Contr.*, vol. 42, no. 7, pp. 896-911, 1997.

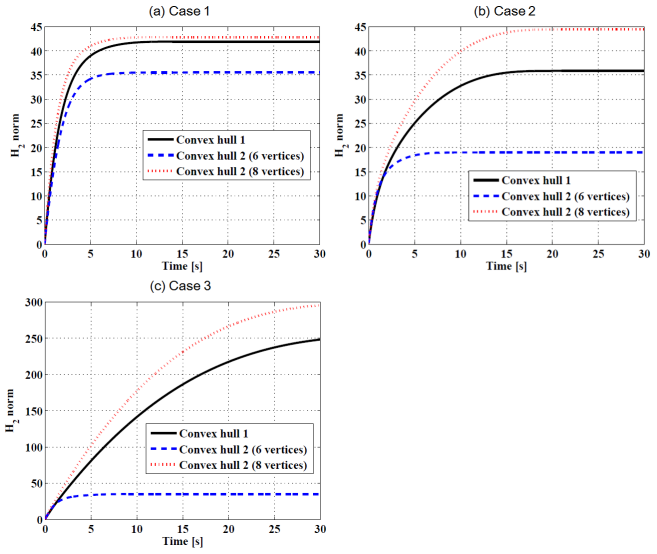

Fig. 6. $\mathcal{H}_2$ norms.

[11] P. Apkarian and R. J. Adams, "Advanced gain-scheduled techniques for uncertain systems," *IEEE Trans. on Contr. Sys. Tech.*, vol. 6, no. 1, pp. 21-32, 1998.

[12] E. Feron, P. Apkarian, and P. Gahinet, "Analysis and synthesis of robust control systems via parameter-dependent Lyapunov functions," *IEEE Trans. on Automat. Contr.*, vol. 41, no. 7, pp. 1041-1046, 1996.

[13] P. Gahinet, P. Apkarian, and M. Chilali, "Affine parameter-dependent Lyapunov functions and real parametric uncertainty," *IEEE Trans. on Automat. Contr.*, vol. 41, no. 3, pp. 436-442, 1996.

[14] F. Wu, X. H. Yang, A. Packard and G. Becker, "Induced L_2-norm control for LPV system with bounded parameter variation rates," *Proc. American Contr. Conf.*, pp. 2379-2383, 1995.

[15] T. Shimomura and T. Kubotani, "Gain-Scheduled Control under Common Lyapunov Functions: Conservatism Revisited," *Proc. American Contr. Conf.*, pp. 870-875, 2005.

[16] T. Shimomura and T. Fujii, "Multiobjective control via successive over-bounding of quadratic terms," *Int. J. Robust Nonlin. Contr.*, vol. 15, no. 8, pp. 363-381, 2005.

[17] R. Watanabe, K. Uchida, and M. Fujita, "A New LMI Approach to Analysis of Linear Systems with Scheduling Parameter-Reduction to Finite Number of LMI Conditions-," *Proc. IEEE Conf. Decision Contr.,* pp. 1663-1665, 1996.

[18] A. Kwiatkowski, S. Trimpe and H. Werner, "Less Conservative Polytopic LPV Models for Charge Controlby Combining Parameter Set Mapping and Set Intersection," *Proc. IEEE Conf. Decision Contr.,* pp. 3363-3368, 2007.

[19] A. Kwiatkowski and H. Werner, "PCA-Based Parameter Set Mappings for LPV Models With Fewer Parameters and Less Overbounding," *IEEE Trans. on Contr. Systems Technology*, Vol. 16, No. 4, July, 2008.

[20] T. Azuma, R. Watanabe, K. Uchida, and M. Fujita, "A New LMI Approach to Analysis of Linear Systems Depending on Scheduling Parameter in Polynomial Forms," *Automatisierungstechnik*, Vol. 48, 2000.

[21] T. Shimomura, "Hybrid control of gain-scheduling and switching: a design example of aircraft control," *Proc. American Contr. Conf.*, pp. 4639-4644, 2003.

[22] M. Chilali and P. Gahinet, "H_∞ Design with Pole Placement Constraints: An LMI Approach," *IEEE Trans. on Automat. Contr.*, vol. 41, no. 3, pp. 358-367, 1996.

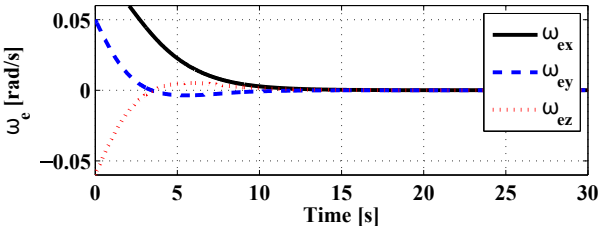

(a) Angular velocity (state variable)

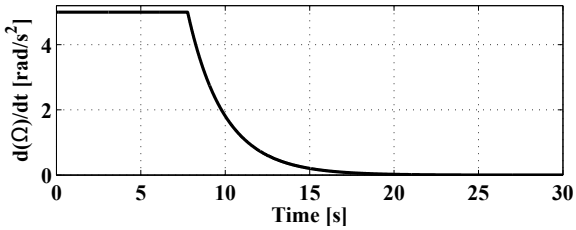

(b) Wheel acceleration (wheel input)

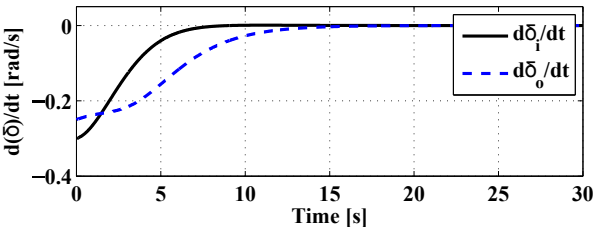

(c) Gimbal rates (gimbal input)

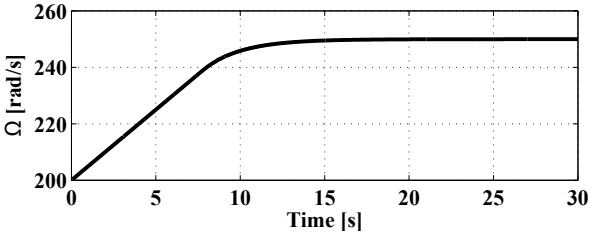

(d) Wheel spin rate

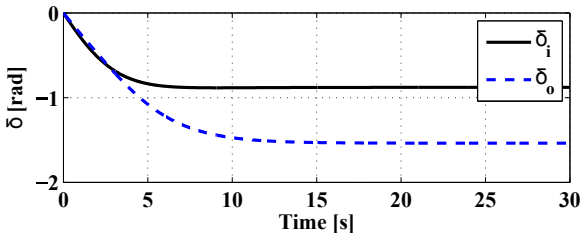

(e) Gimbal angles

Fig. 7. Attitude stabilization: Convex hull #1 (Case 1).